NANO LETTERS

pubs.acs.org/NanoLett Letter

In Situ Ni^{2+} Stain for Liposome Imaging by Liquid-Cell Transmission Electron Microscopy

Karthikeyan Gnanasekaran, HanByul Chang, Paul J. M. Smeets, Joanna Korpanty, Franz M. Geiger,* and Nathan C. Gianneschi*

Cite This: *Nano Lett.* 2020, 20, 4292–4297 Read Online

ACCESS | Metrics & More | Article Recommendations | Supporting Information

ABSTRACT: Solvated soft matter, both biological and synthetic, can now be imaged in liquids using liquid-cell transmission electron microscopy (LCTEM). However, such systems are usually composed solely of organic molecules (low *Z* elements) producing low contrast in TEM, especially within thick liquid films. We aimed to visualize liposomes by LCTEM rather than requiring cryogenic TEM (cryoTEM). This is achieved here by imaging in the presence of aqueous metal salt solutions. The increase in scattering cross-section by the cation gives a staining effect that develops *in situ*, which could be captured by real space TEM and verified by *in situ* energy dispersive x-ray spectroscopy (EDS). We identified beam-induced staining as a time-dependent process that enhances contrast to otherwise low contrast materials. We describe the development of this imaging method and identify conditions leading to exceptionally low electron doses for morphology visualization of unilamellar vesicles before beam-induced damage propagates.

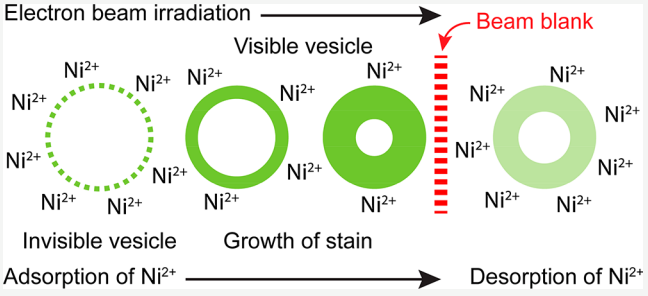

KEYWORDS: *Liposomes, liquid-phase TEM, in situ EDS, in situ staining, contrast enhancement, image analysis*

Liquid-cell transmission electron microscopy (LCTEM) is under development for the study of dynamics, growth kinetics, and reactivity of nanomaterials with the majority of work focused on inorganic nanoparticles.[1−6] However, LCTEM of soft materials is challenging because they are largely comprised of low-atomic number elements that produce little contrast and are sensitive toward electron beam induced radiation damage.[7−11] In addition, thick liquid samples result in electron beam broadening and relatively high background signals that decrease image contrast and resolution.[12,13] In classical TEM, contrast produced by density variation is enhanced by selective staining between the phases of the material.[14−16] In LCTEM, Piffoux et al. reported the electron beam induced reduction of chloroauric acid to Au metal nanoparticles on extracellular vesicle membranes, which enhances the image contrast.[17]

Here, we propose the use of a standard metal salt ($NiCl_2$) as a reversible *in situ* stain for lipopolysaccharides, a common lipid and major constituent of Gram-negative bacterial cell walls.[18] We are motivated by our recent finding that Ni^{2+} ions bind largely reversibly to the O-antigen of smooth lipopolysaccharides (sLPS, Figure 1, and Figure S1), presumably through complexation with their negatively charged carboxylic acid groups, with coverages of around 1×10^{13} Ni^{2+} ions adsorbed cm^{-2} and a free binding constant of around −28 kJ mol^{-1} (Figure 1A).[19] CryoTEM shows that vesicles formed from a mix of O-antigen-containing sLPS and the zwitterionic lipid 1-palmitoyl-2-oleoyl-*sn*-glycero-3-phosphocholine (POPC) resist deformation upon Ni^{2+} binding even in the presence of 100 mM $NiCl_2$ (Figure S2). Therefore, we reason that selective reversible staining of lipid membranes should be possible with Ni salts.

To test our hypothesis, we performed LCTEM of POPC-sLPS vesicles in the presence of aqueous $NiCl_2$ solution (see Supporting Information, Sections SI−SV for sample preparation and experimental details). We recorded the LCTEM video frames at various electron fluxes and $NiCl_2$ concentrations. In the absence of Ni salt, vesicles are not visible for the first 60 s when using a flux of 0.15 e^- $Å^{-2}$ s^{-1} (Figure 1B, Movie S1). Prolonged exposure of ∼20 min (cumulative dose of ∼200 $e^-Å^{-2}$) leads to the appearance of round structures having a diameter commensurate with the size of the vesicles (∼100 nm) whose centers feature spots of several tens of nm in size that become increasingly dark and aggregates as exposure time progresses (Figure S4A and Movie S2). By increasing the electron flux to 0.4 e^- $Å^{-2}$ s^{-1}, we immediately observe the vesicles with distinct spots in the membrane indicating damage

Received: February 29, 2020
Revised: May 5, 2020
Published: May 26, 2020

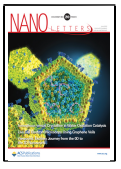

https://dx.doi.org/10.1021/acs.nanolett.0c00898
Nano Lett. 2020, 20, 4292–4297

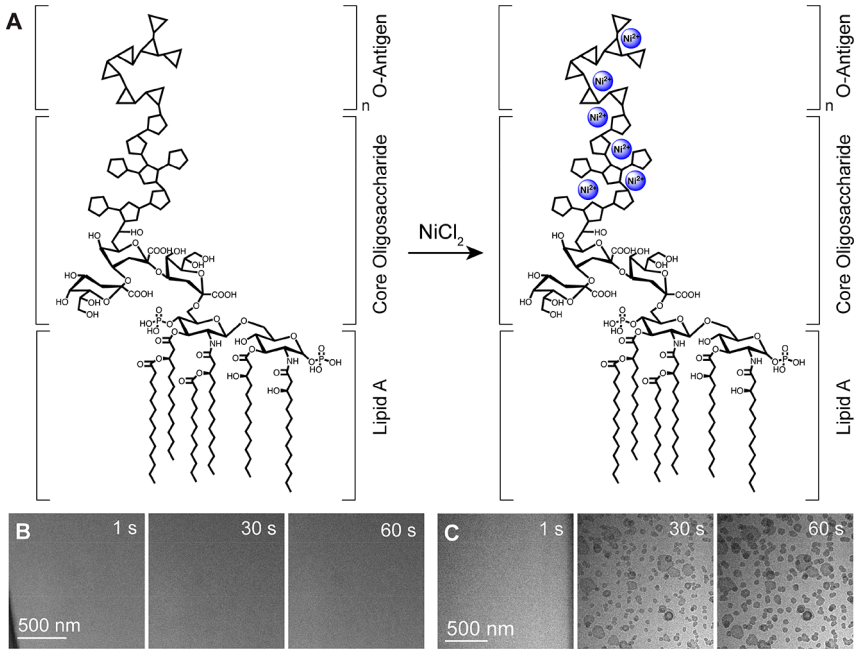

Figure 1. (A) Schematic depiction of the molecular structure of POPC-sLPS and POPC-sLPS with Ni^{2+} complexation. (B) LCTEM frames of POPC-sLPS vesicles without aqueous $NiCl_2$ solution acquired with an electron flux of 0.15 e^- $Å^{-2}$ s^{-1}. (C) LCTEM frames of POPC-sLPS vesicles with 1 mM aqueous $NiCl_2$ solution acquired with an electron flux of 0.2 e^- $Å^{-2}$ s^{-1}.

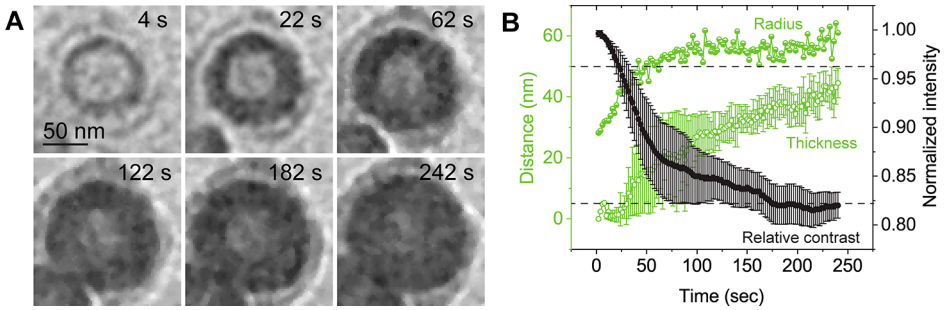

Figure 2. Quantitative analysis of POPC-sLPS vesicles measured by LCTEM. (A) Snapshots of aligned and averaged filtered vesicle at various time points. Images are cropped from Movie S5. (B) Radius and stain thickness, normalized intensity of POPC-sLPS vesicles with 1 mM aqueous $NiCl_2$ solution acquired with an electron flux of 0.2 e^- $Å^{-2}$ s^{-1} as a function of time. Black dotted line represents the typical membrane thickness (~5 nm) and radius (~50 nm) of POPC-sLPS vesicles measured by cryoTEM.

by the electron beam (Figure S4C, Movie S3, and Movie S4). In contrast to the nickel-free solutions, POPC-sLPS vesicles are visible at electron fluxes as low as 0.2 e^- $Å^{-2}$ s^{-1} when 1 mM $NiCl_2$ is present (Figure 1C and Movie S5, Movie S6, Movie S7. We attribute the significant contrast to the scattering cross section of Ni^{2+} ions complexed with the negatively charged carboxylic acid groups of POPC-sLPS.[19,20] The vesicle stain intensifies at about 60 s, after which the fully stained image in the LCTEM is comparable to that in cryoTEM (~100 nm in diameter). Higher $NiCl_2$ concentrations (10 and 100 mM) result in overstaining (Figure S5 and Movies S8–S11) and swelling that may be attributed to Ni^{2+} mediated beam-induced reactions or charge reversal of the membranes from negative to highly positive that coincides with high [Ni^{2+}] (Figure S6).[21] The change in membrane stain thickness, the apparent size of the vesicles, and relative contrast during staining are quantified (for detailed information on image analysis see Supporting Information Section X and XI, Figures S7– S10).[11] In contrast to the unstained vesicles (Figure 1B), staining leads to gradual increases in thickness, radius, and contrast of the imaged objects until a constant size is reached (Figure 2). Higher concentrations of $NiCl_2$ solution (100 mM) lead to drastic growth in the stain size and affects the image contrast (see Supporting Information Section XII, Figure S11 and Figure S12).

To examine the dynamics of the stain buildup (Figure 3), we estimated the amount of unbound, free Ni^{2+} in the aqueous solution during the first few minutes of imaging (Figure 3A). Here, the concentration of free Ni^{2+} ions in aqueous solution is related to the change in mean background intensity, and thus the change in mean free path of the electron at every frame over a constant liquid thickness (see Supporting Information, Section XIII). Our analysis shows ~70% of the free Ni^{2+} ions present in the 1 mM $NiCl_2$ solution in the liquid cell is lost during the first 200 s of irradiation (Figure 3B, Figure S13, Movie S5), presumably to the vesicles. Following a 2 min beam blank, the free Ni^{2+} ion abundance returns close to 100%, while the image contrast is considerably less than what it was prior to blanking the beam (Figure 3C). However, further irradiation (i.e., second and third irradiation phase) does not initiate the

https://dx.doi.org/10.1021/acs.nanolett.0c00898
Nano Lett. 2020, 20, 4292–4297

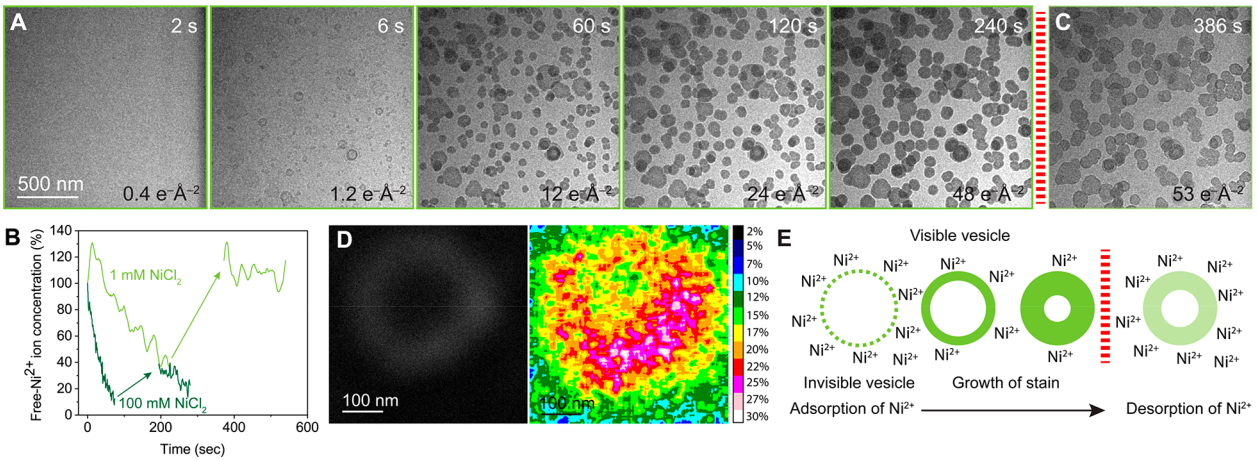

Figure 3. Partial reversibility of stain. (A) Snapshots of POPC-sLPS vesicles with 1 mM $NiCl_2$ as a function of time and cumulative dose. Red strip represents a time period of 120 s where the electron beam is turned off. (B) Free Ni^{2+} ion concentration (%) quantified from background intensity as a function of irradiation time. Arrows indicate the shift in free Ni^{2+} ion concentration during the beam blank period of 120 s. (C) A snapshot in the beginning of the 2nd phase of electron beam irradiation illustrates the decrease in relative contrast. (D) HAADF-STEM image and the corresponding atomic percent of Ni in situ EDS map of a vesicle with 100 mM $NiCl_2$ solution. (E) Schematic illustration of partial reversible interaction of Ni^{2+} ions with vesicles.

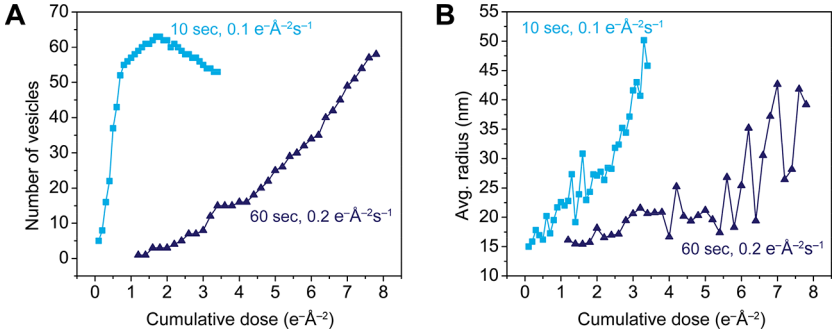

Figure 4. (A) Visible number of POPC-sLPS vesicles with 1 mM $NiCl_2$ solution and (B) the average radius measured over time as a function of cumulative electron dose for various acquisition conditions.

growth of membrane stain as the background intensity remains almost constant over the entire irradiation phase. As expected, prolonged exposure (i.e., at higher cumulative doses) leads to beam-induced fusion and coalescence in the imaged structures (Figure S13A, Movie S6, Movie S7). The constant background intensity in the second phase of irradiation suggests that diffusion of Ni^{2+} ions (i.e., adsorption and desorption) is not the only effect altering background intensity. It has been reported that prolonged irradiation leads to the formation of gas bubbles and changes in local supersaturation, resulting from radiolysis reactions, which could alter the liquid thickness and background intensity and thus influence any estimation of free-Ni^{2+} ion concentrations.[22,23] However, when using 100 mM $NiCl_2$ solutions, the rate of initial adsorption of free-Ni^{2+} ions is significantly faster as compared to when 1 mM $NiCl_2$ solutions are used. Subsequent desorption leads to 40% recovery of free-Ni^{2+} ions (Figure 3B and Figure S13, Movie S9, Movie S10, Movie S11). This difference in behavior of Ni^{2+} ions at 1 and 100 mM $NiCl_2$ shows that changes in the background intensity are predominantly affected by the concentration of the $NiCl_2$.

While the mechanism underlying the observed staining processes needs to be elucidated, it is likely that solvent radiolysis byproducts (predominately e^-_{aq}, $^{\bullet}OH$) attack organic functional groups in the liposomes.[24,25] It has been shown that amino acids are prone to attack by $^{\bullet}OH$ radicals leading to hydrogen abstraction at the α-C position to −COOH groups.[26] $^{\bullet}OH$ radicals induce oxidative degradation of lipids (such as lipid peroxidation). This leads to the formation of radical intermediates and radical anions on the organic molecules. In turn, this causes unbound free-Ni^{2+} to localize at the charged negative groups, leading to an increase in the thickness of the stain with time in the membranes. By blanking the beam, deexcitation of this dynamic process leads to expulsion of excess Ni^{2+} ions.[24,25,27−29] The effects of beam-induced radiolysis and osmotic pressure are discussed further in the Supporting Information Sections XIII and XVI.[24,25,27−30]

In situ energy dispersive X-ray spectroscopy (*in situ* EDS) at a controlled electron dose (see Supporting Information Section SXIV) provides chemical evidence of the accumulation of Ni^{2+} ions at vesicle membranes (Figure 3D), identifying Ni coverages of 7 ± 3% and 14 ± 4% at 10 and 100 mM $NiCl_2$, respectively (Figure S14), comparable to our earlier estimates from second harmonic generation (Figure S16).[19] Flowing buffer solution through the liquid-cell holder and around the tip assembly leads to desorption of Ni^{2+} ions where the residual Ni^{2+} accounts for 5 ± 2% and 9 ± 5% at 10 and 100 mM $NiCl_2$ samples, respectively. On the basis of reversibility of free Ni^{2+} ion and residual Ni^{2+} ions on the vesicles, we conclude that the

https://dx.doi.org/10.1021/acs.nanolett.0c00898
Nano Lett. 2020, 20, 4292−4297

Ni^{2+} stain is partially reversible (cartoon depiction of this process in Figure 3E). Our experiments highlight the importance of the Ni^{2+} concentration, the loss rate of those ions from the solution to the vesicles, electron flux, and the total cumulative dose as parameters to consider. Indeed, it is likely that prolonged electron beam exposure leads to the reduction of Ni^{2+} to Ni^0, followed by nucleation, and partial oxidation to form Ni/NiO nanoparticles.[5,6,21,31−33] Nevertheless, X-ray photoelectron spectroscopy (XPS) analysis on LCTEM chips pried open and dried after *in situ* imaging reveals the dominant metal speciation to be Ni^{2+} on the localized irradiated region (Figure S17). We observe no Ni^0 where the cumulative electron doses remain less than ∼200 $e^-Å^{-2}$.

To assess the minimum cumulative dose required for usable image contrast, we imaged for a duration of 1 s at a given electron flux and blanked the beam for up to 1 min, followed by subsequent repeat measurements to sample up to ∼8 e^- $Å^{-2}$. We observe that a beam blank duration of 10 s combined with a flux of 0.1 e^- $Å^{-2}$ s^{-1} reveal >50 vesicles at their cryoTEM derived radii (∼50 nm) at a cumulative dose of just 3 e^- $Å^{-2}$ (Figure 4, Figure S18, Figure S19, and Movies S12−S14). This low cumulative dose needed to image soft matter in LCTEM provides clear evidence of the potential utility of the Ni^{2+} stain identified here. In contrast, beam blank durations of 1 min, even at twice the flux, require considerably larger cumulative doses. We also identified that depending on the imaging requirement, that is, static imaging (for a short period of time) or dynamic imaging (for a long period of time), the electron flux and concentration of $NiCl_2$ solutions can be manipulated to minimize the total accumulated dose (see Supporting Information Section SXII).

In conclusion, we have shown that vesicles formed from lipopolysaccharides can be readily stained *in situ* with Ni^{2+} ions in a partially reversible fashion. The staining is shown to depend on the Ni^{2+} ion concentration, the electron dose conditions, and the electron beam duty cycle when imaging using a pulsed electron beam with beam blank intervals. Moreover, we showed that low contrast soft materials can be visualized well before beam-induced artifacts and damage occur. Specifically, we determined that low metal salt concentrations (≤1 mM $NiCl_2$) and low electron fluxes (i.e., 0.1−0.2 e^- $Å^{-2}$ s^{-1}) are sufficient for imaging vesicles out to their cryoTEM-derived radius at cumulative doses of as little as 3 $e^-Å^{-2}$. We note that for LCTEM, contrast is a problem due to a lack of control of liquid thickness. Staining approaches can overcome these contrast problems that arise because of the low doses required. More generally, our approach opens up the possibility of LCTEM being a routine tool complementing cryoTEM for characterizing soft matter. This could be particularly interesting when capturing dynamics and in addition for imaging systems solvated in organic solvents not commonly employed in cryoTEM. Though prolonged staining would perturb the dynamics of the system, periodic staining via optimized partial reversible staining strategies could allow dynamic processes to be observed using LCTEM. The experiments reported here also open the possibility to synthesize hard materials on the soft templated architectures.[34−36] More importantly, morphological characterization of soft matter, with judicious choice of metal stain provides a facile route to morphological characterization of solvated soft matter.

■ ASSOCIATED CONTENT

Supporting Information

The Supporting Information is available free of charge at https://pubs.acs.org/doi/10.1021/acs.nanolett.0c00898.

Sample preparation, cryoTEM images, LCTEM experimental details, electron flux measurements, liquid thickness measurements, LCTEM control experiments, Zeta potential measurements, image analysis, additional quantitative analysis, discussion on dynamics of Ni^{2+} staining, quantification of background intensity, additional *in situ* EDS data, SHG spectroscopy, radiolysis reactions, XPS data, minimum dose requirement for stained LCTEM imaging (PDF)

sifile1

LCTEM data of POPC-sLPS vesicles acquired with an electron flux of 0.15 e^- $Å^{-2}$ s^{-1} (AVI)

LCTEM movie shows the degradation of POPC-sLPS by prolonged electron beam exposure of ∼20 min. Data acquired with an electron flux of 0.15 e^- $Å^{-2}$ s^{-1} (AVI)

LCTEM data of POPC-sLPS vesicles acquired with an electron flux of 0.3 e^- $Å^{-2}$ s^{-1} (AVI)

LCTEM data of POPC-sLPS vesicles acquired with an electron flux of 0.4 e^- $Å^{-2}$ s^{-1} (AVI)

LCTEM data of POPC-sLPS vesicles with 1 mM aqueous $NiCl_2$ solution acquired with an electron flux of 0.2 e^- $Å^{-2}$ s^{-1}. 1st phase imaging. (AVI)

LCTEM data of POPC-sLPS vesicles with 1 mM aqueous $NiCl_2$ solution acquired with an electron flux of 0.2 e^- $Å^{-2}$ s^{-1}. 2nd phase imaging after 120 s of beam blank (AVI)

LCTEM data of POPC-sLPS vesicles with 1 mM aqueous $NiCl_2$ solution acquired with an electron flux of 0.2 e^- $Å^{-2}$ s^{-1}. 3rd phase imaging after 120 s beam blank (AVI)

LCTEM data of POPC-sLPS vesicles with 10 mM aqueous $NiCl_2$ solution acquired with an electron flux of 0.2 e^- $Å^{-2}$ s^{-1} (AVI)

LCTEM data of POPC-sLPS vesicles with 100 mM aqueous $NiCl_2$ solution acquired with an electron flux of 0.2 e^- $Å^{-2}$ s^{-1}. 1st phase imaging (AVI)

LCTEM data of POPC-sLPS vesicles with 100 mM aqueous $NiCl_2$ solution acquired with an electron flux of 0.2 e^- $Å^{-2}$ s^{-1}. 2nd phase imaging after 120 s beam blank (AVI)

LCTEM data of POPC-sLPS vesicles with 100 mM aqueous $NiCl_2$ solution acquired with an electron flux of 0.2 e^- $Å^{-2}$ s^{-1}. 3rd phase imaging after 120 s beam blank (AVI)

LCTEM data of POPC-sLPS vesicles with 1 mM aqueous $NiCl_2$ solution acquired with an electron flux of 0.1 e^- $Å^{-2}$ s^{-1} and time interval of 10 s (AVI)

LCTEM data of POPC-sLPS vesicles with 1 mM aqueous NiCl2 solution acquired with an electron flux of 0.2 e^- $Å^{-2}$ s^{-1} and time interval of 30 s (AVI)

LCTEM data of POPC-sLPS vesicles with 1 mM aqueous $NiCl_2$ solution acquired with an electron flux of 0.2 e^- $Å^{-2}$ s^{-1} and time interval of 60 s (AVI)

■ AUTHOR INFORMATION

Corresponding Authors

Nathan C. Gianneschi − *Department of Chemistry and Department of Materials Science and Engineering, Northwestern*

https://dx.doi.org/10.1021/acs.nanolett.0c00898
Nano Lett. 2020, 20, 4292−4297

University, Evanston, Illinois 60208, United States; International Institute for Nanotechnology, Evanston, Illinois 60208, United States; Department of Biomedical Engineering, Pharmacology, Simpson-Querrey Institute, Chemistry of Life Processes Institute, Evanston, Illinois 60208, United States; orcid.org/0000-0001-9945-5475; Email: nathan.gianneschi@northwestern.edu

Franz M. Geiger − *Department of Chemistry, Northwestern University, Evanston, Illinois 60208, United States; International Institute for Nanotechnology, Evanston, Illinois 60208, United States;* orcid.org/0000-0001-8569-4045; Email: geigerf@chem.northwestern.edu

Authors

Karthikeyan Gnanasekaran − *Department of Chemistry, Northwestern University, Evanston, Illinois 60208, United States; International Institute for Nanotechnology, Evanston, Illinois 60208, United States;* orcid.org/0000-0001-6635-0888

HanByul Chang − *Department of Chemistry, Northwestern University, Evanston, Illinois 60208, United States; International Institute for Nanotechnology, Evanston, Illinois 60208, United States*

Paul J. M. Smeets − *International Institute for Nanotechnology, Evanston, Illinois 60208, United States; Department of Materials Science and Engineering and NUANCE Center, Northwestern University, Evanston, Illinois 60208, United States;* orcid.org/0000-0002-7281-0120

Joanna Korpanty − *Department of Chemistry, Northwestern University, Evanston, Illinois 60208, United States; International Institute for Nanotechnology, Evanston, Illinois 60208, United States*

Complete contact information is available at: https://pubs.acs.org/10.1021/acs.nanolett.0c00898

Author Contributions

K.G. designed the study, conducted all the LCTEM experiments, *in situ* STEM-EDS, cryoTEM imaging, image analysis, and wrote the manuscript. H.C. participated in the sample preparation, performed SHG, DLS, Zeta potential measurements. P.J.M.S. participated in collecting *in situ* EDS data. J.K. conducted the XPS measurements on LCTEM chips. F.M.G. and N.C.G. supervised all research phases and revised the manuscript. All the authors discussed and commented on the manuscript.

Notes

The authors declare no competing financial interest.

■ ACKNOWLEDGMENTS

This research used EPIC facility of Northwestern University's NUANCE Center, which has received support from the Soft and Hybrid Nanotechnology Experimental (SHyNE) Resource (NSF ECCS-1542205); the MRSEC program (NSF DMR-1720139) at the Materials Research Center; the International Institute for Nanotechnology (IIN); the Keck Foundation; and the State of Illinois, through the IIN. Furthermore, we thank the Army Research Office (W911NF-17-1-0326, MURI W911NF-15-1-0568) and the National Science Foundation (CHE-1905270) for support. K.G. is appreciative of a postdoctoral fellowship from the Human Frontier Science Program (LT000869/2018-C). This work is supported by the National Science Foundation under the Center for Sustainable Nanotechnology, Grant CHE-1503408. F.M.G. acknowledges support from a Dow Chemical Company Professorship and from the Alexander von Humboldt Foundation.

■ REFERENCES

(1) Ross, F. M. Opportunities and challenges in liquid cell electron microscopy. *Science* **2015**, *350* (6267), aaa9886.
(2) de Jonge, N.; Ross, F. M. Electron microscopy of specimens in liquid. *Nat. Nanotechnol.* **2011**, *6* (11), 695−704.
(3) Yuk, J. M.; Park, J.; Ercius, P.; Kim, K.; Hellebusch, D. J.; Crommie, M. F.; Lee, J. Y.; Zettl, A.; Alivisatos, A. P. High-resolution EM of colloidal nanocrystal growth using graphene liquid cells. *Science* **2012**, *336* (6077), 61−4.
(4) Nielsen, M. H.; Aloni, S.; De Yoreo, J. J. In situ TEM imaging of CaCO(3) nucleation reveals coexistence of direct and indirect pathways. *Science* **2014**, *345* (6201), 1158−62.
(5) Woehl, T. J.; Evans, J. E.; Arslan, I.; Ristenpart, W. D.; Browning, N. D. Direct in situ determination of the mechanisms controlling nanoparticle nucleation and growth. *ACS Nano* **2012**, *6* (10), 8599−610.
(6) Evans, J. E.; Jungjohann, K. L.; Browning, N. D.; Arslan, I. Controlled growth of nanoparticles from solution with in situ liquid transmission electron microscopy. *Nano Lett.* **2011**, *11* (7), 2809−13.
(7) Parent, L. R.; Bakalis, E.; Ramirez-Hernandez, A.; Kammeyer, J. K.; Park, C.; de Pablo, J.; Zerbetto, F.; Patterson, J. P.; Gianneschi, N. C. Directly Observing Micelle Fusion and Growth in Solution by Liquid-Cell Transmission Electron Microscopy. *J. Am. Chem. Soc.* **2017**, *139* (47), 17140−17151.
(8) Patterson, J. P.; Abellan, P.; Denny, M. S., Jr.; Park, C.; Browning, N. D.; Cohen, S. M.; Evans, J. E.; Gianneschi, N. C. Observing the growth of metal-organic frameworks by in situ liquid cell transmission electron microscopy. *J. Am. Chem. Soc.* **2015**, *137* (23), 7322−8.
(9) Proetto, M. T.; Rush, A. M.; Chien, M. P.; Abellan Baeza, P.; Patterson, J. P.; Thompson, M. P.; Olson, N. H.; Moore, C. E.; Rheingold, A. L.; Andolina, C.; Millstone, J.; Howell, S. B.; Browning, N. D.; Evans, J. E.; Gianneschi, N. C. Dynamics of soft nanomaterials captured by transmission electron microscopy in liquid water. *J. Am. Chem. Soc.* **2014**, *136* (4), 1162−5.
(10) Vailonis, K. M.; Gnanasekaran, K.; Powers, X. B.; Gianneschi, N. C.; Jenkins, D. M. Elucidating the Growth of Metal-Organic Nanotubes Combining Isoreticular Synthesis with Liquid-Cell Transmission Electron Microscopy. *J. Am. Chem. Soc.* **2019**, *141* (26), 10177−10182.
(11) Ianiro, A.; Wu, H.; van Rijt, M. M. J.; Vena, M. P.; Keizer, A. D. A.; Esteves, A. C. C.; Tuinier, R.; Friedrich, H.; Sommerdijk, N.; Patterson, J. P. Liquid-liquid phase separation during amphiphilic self-assembly. *Nat. Chem.* **2019**, *11* (4), 320−328.
(12) Keskin, S.; Kunnas, P.; de Jonge, N. Liquid-Phase Electron Microscopy with Controllable Liquid Thickness. *Nano Lett.* **2019**, *19* (7), 4608−4613.
(13) de Jonge, N.; Poirier-Demers, N.; Demers, H.; Peckys, D. B.; Drouin, D. Nanometer-resolution electron microscopy through micrometers-thick water layers. *Ultramicroscopy* **2010**, *110* (9), 1114−9.
(14) Kato, K. The osmium tetroxide procedure for light and electron microscopy of ABS plastics. *Polym. Eng. Sci.* **1967**, *7* (1), 38−39.
(15) Hobbs, S. Y. Polymer Microscopy. *J. Macromol. Sci., Polym. Rev.* **1980**, *C19* (2), 221−265.
(16) Alfert, M.; Geschwind, II A Selective Staining Method for the Basic Proteins of Cell Nuclei. *Proc. Natl. Acad. Sci. U. S. A.* **1953**, *39* (10), 991−9.
(17) Piffoux, M.; Ahmad, N.; Nelayah, J.; Wilhelm, C.; Silva, A.; Gazeau, F.; Alloyeau, D. Monitoring the dynamics of cell-derived extracellular vesicles at the nanoscale by liquid-cell transmission electron microscopy. *Nanoscale* **2018**, *10* (3), 1234−1244.
(18) Cornelissen, G.; van Noort, P. C. M.; Govers, H. A. J. Mechanism of slow desorption of organic compounds from

sediments: a study using model sorbents. *Environ. Sci. Technol.* **1998**, *32*, 3124−3131.
(19) Chang, H.; Gnanasekaran, K.; Gianneschi, N. C.; Geiger, F. M. Bacterial Model Membranes Deform (resp. Persist) upon Ni(2+) Binding to Inner Core (resp. O-Antigen) of Lipopolysaccharides. *J. Phys. Chem. B* **2019**, *123* (19), 4258−4270.
(20) Bala, T.; Prasad, B. L.; Sastry, M.; Kahaly, M. U.; Waghmare, U. V. Interaction of different metal ions with carboxylic acid group: a quantitative study. *J. Phys. Chem. A* **2007**, *111* (28), 6183−90.
(21) Woehl, T. J.; Abellan, P. Defining the radiation chemistry during liquid cell electron microscopy to enable visualization of nanomaterial growth and degradation dynamics. *J. Microsc.* **2017**, *265* (2), 135−147.
(22) Abellan, P.; Woehl, T. J.; Parent, L. R.; Browning, N. D.; Evans, J. E.; Arslan, I. Factors influencing quantitative liquid (scanning) transmission electron microscopy. *Chem. Commun. (Cambridge, U. K.)* **2014**, *50* (38), 4873−80.
(23) Jiang, N. Note on in situ (scanning) transmission electron microscopy study of liquid samples. *Ultramicroscopy* **2017**, *179*, 81−83.
(24) Bhattacharyya, S. N.; Kundu, K. P. On the radiolysis of aqueous solutions of nickel (II) ethylenediamine tetraacetate. *Radiat. Res.* **1972**, *51* (1), 45−55.
(25) Bhattacharyya, S. N.; Kundu, K. P. X-Irradiation of Aqueous-Solutions of Ethylenediamine Tetraacetic Acid (Edta). *Int. J. Radiat. Phys. Chem.* **1972**, *4* (1), 31−41.
(26) Willix, R. L.; Garrison, W. M. Chemistry of the hydrated electron in oxygen-free solutions of amino acids, peptides, and related compounds. *Radiat. Res.* **1967**, *32* (3), 452−62.
(27) Srisankar, E. V.; Bhattacharyya, S. N. Pulse and γ-radiolysis of nickel(II) nitrilotriacetate in aqueous solutions. *J. Chem. Soc., Dalton Trans.* **1980**, *4*, 675−680.
(28) Sellers, R. M. Metal-Ions in Unusual Valency States. *J. Chem. Educ.* **1981**, *58* (2), 114−118.
(29) Buxton, G. V.; Sellers, R. M. The radiation chemistry of metal ions in aqueous solution. *Coord. Chem. Rev.* **1977**, *22* (3), 195−274.
(30) Schneider, N. M.; Norton, M. M.; Mendel, B. J.; Grogan, J. M.; Ross, F. M.; Bau, H. H. Electron−Water Interactions and Implications for Liquid Cell Electron Microscopy. *J. Phys. Chem. C* **2014**, *118* (38), 22373−22382.
(31) Zhang, Y.; Keller, D.; Rossell, M. D.; Erni, R. Formation of Au Nanoparticles in Liquid Cell Transmission Electron Microscopy: From a Systematic Study to Engineered Nanostructures. *Chem. Mater.* **2017**, *29* (24), 10518−10525.
(32) Liu, Y.; Tai, K. P.; Dillon, S. J. Growth Kinetics and Morphological Evolution of ZnO Precipitated from Solution. *Chem. Mater.* **2013**, *25* (15), 2927−2933.
(33) Wang, Y.; Wang, S.; Lu, X. In Situ Observation of the Growth of ZnO Nanostructures Using Liquid Cell Electron Microscopy. *J. Phys. Chem. C* **2018**, *122* (1), 875−879.
(34) Pal, N.; Bhaumik, A. Soft templating strategies for the synthesis of mesoporous materials: inorganic, organic-inorganic hybrid and purely organic solids. *Adv. Colloid Interface Sci.* **2013**, *189−190*, 21−41.
(35) Zhu, C.; Du, D.; Eychmuller, A.; Lin, Y. Engineering Ordered and Nonordered Porous Noble Metal Nanostructures: Synthesis, Assembly, and Their Applications in Electrochemistry. *Chem. Rev.* **2015**, *115* (16), 8896−943.
(36) Dong, R.; Liu, W.; Hao, J. Soft vesicles in the synthesis of hard materials. *Acc. Chem. Res.* **2012**, *45* (4), 504−13.

https://dx.doi.org/10.1021/acs.nanolett.0c00898
Nano Lett. 2020, 20, 4292−4297